



# Numerical Investigation of Heat Transfer Enhancement in Circular Channel with Variation in Angle of Delta-Winglet Vortex Generator

M Iqbal Farhan Putra Arya<sup>1,\*</sup>, Syaiful<sup>1</sup>, Muchammad<sup>1</sup>, Maria F. Soetanto<sup>2</sup>

<sup>1</sup> Department of Mechanical Engineering, Faculty of Engineering, Diponegoro University, Semarang, Indonesia

<sup>2</sup> Aerospace Department of Polytechnic of Bandung, Bandung, Indonesia

## ARTICLE INFO

### Article history:

Received 30 September 2022

Received in revised form 25 October 2022

Accepted 20 November 2022

Available online 1 March 2023

### Keywords:

delta-winglet vortex generator; heat transfer rate; friction factor; thermal-hydraulic performance

## ABSTRACT

Vortex generators have been used to enhance heat transfer in numerous industries. Vortex generators improve flow mixing by destroying the thermal boundary layer, which improves heat transfer. This study aimed to improve heat transfer in circular channels by installing delta-winglet vortex generators. Accordingly, delta-winglet vortex generators with different angles – 90°, 105°, 120°, 135°, and 150° – were installed in an in-line arrangement. The  $k-\omega$  turbulent SST model was applied to Reynolds numbers ranging from 4,000 to 12,000, varied at an interval of 2,000. The results indicated that a delta-winglet vortex generator with an angle of 90° increased heat transfer by 4.05% compared to that with an angle of 150°, while the flow resistance also increased by 7.18%. The delta-winglet vortex generator with an angle of 90° achieved the highest thermal enhancement factor of 2.55, whereas that with an angle of 150° provided the lowest cost-benefit ratio of 0.61.

## 1. Introduction

Heat exchangers with vortex generators (VGs) are increasingly being used in manufacturing owing to their ability to effectively increase heat transfer [1–3]. The installation of VGs can reduce operating costs and increase efficiency in power plants and central cooling rooms. Owing to the increased efficiency of such heat exchangers, they can be designed to be more compact and cheaper [4].

VGs disturb the thermal boundary layer, forming vortices. These vortices cause turbulent flow, which impacts the mixing between hot and cold fluids and increases the heat transfer rate [5–9]. The heat transfer rate is also affected by the surface area of the VG. A VG with a wider frontal area improves heat transfer in the channel [10, 11].

Da Silva *et al.*, [12] evaluated the effects of different VG shapes, using delta winglets (DW) and rectangular winglets (RW) oriented at various angles of attack in circular channels. The results indicated that RW VGs at an angle of attack of 45° provided the highest increase in heat transfer. However, DW VGs at an angle of attack of 30° provided a reasonably small ratio between the heat transfer and pressure drop. Further research was conducted by Luo *et al.*, [13], who optimised the

\* Corresponding author.

E-mail address: [miqbalfarhanpa@gmail.com](mailto:miqbalfarhanpa@gmail.com) (M Iqbal Farhan Putra Arya)

wavy fin attached to DW VGs. The corrugation angle on the wavy fin and the angle of attack of the DW VGs were varied. The results indicated that DW VGs with a corrugation angle of 20° and an angle of attack of 45° were the optimal configuration, as indicated by the high thermo-hydraulic performance. In a subsequent study, Ke *et al.*, [14] investigated and compared a common-flow-up (CFU) and common-flow-down (CFD) configuration in a rectangular channel. The aim of their study was to predict the longitudinal vortex (LV) produced by DW VGs in each configuration. The results indicated that the DW VG in the CFU configuration produced higher LVs than the other configurations because the vortices produced on the lower channel wall forced the vortices to move towards each other, thereby strengthening the LV along the channel.

Lin *et al.*, [15] investigated the performance of VGs with a curved delta winglet (CDW) shape at Reynolds numbers (Re) of 1,100, 1,500, 2,000, 2,500, and 3,000. The results indicated that the CDW VGs provided optimal performance at Re = 3,000, with a thermal enhancement factor (TEF) of 1.35 compared to a plain fin. Luo *et al.*, [16] experimentally investigated heat transfer in a U-duct with DW VGs at various angles of attack – 30°, 45°, 60°, and 90°. The results indicated that an angle of attack of 45° provided optimal thermal–hydraulic performance, which was characterised by an increase in performance by 24% compared to the smooth U-channel. In a subsequent study, Zhao *et al.*, [17] built on the research of Luo *et al.*, [16] by varying the spacing and aspect ratios (ARs) of the DW VGs, and performed numerical simulations to evaluate their performance. They observed that a spacing of 20 mm and an AR of 2 was the optimal design. Perez *et al.*, [18] studied the effects of VG mounting by varying the mounting position, angle of attack, temperature changes, and pressure drop. Their results indicated that a smaller AR impacts heat transfer. This can be attributed to the wider cross-sectional area of a VG with a lower AR. Syaiful *et al.*, [19] evaluated the performance of VGs with two configurations of convex strips – four convex strips and eight convex strips with tubes. The results indicated that eight convex strips produce higher LVs than four convex strips, with a 44% increase in the convection coefficient compared to VGs without convex strips.

Despite this wealth of research, studies on DW VG geometries with different angles are rare. Therefore, in this study, we analyse the effect of various angles of DW VGs installed on a flat plate positioned in the middle of a circular channel. The Nusselt number characteristics of each configuration are used as one of the parameters to identify the heat enhancement effect. Furthermore, the flow resistance is measured by considering the friction factor of each configuration and the Reynolds number.

The novelty of this study is emphasised by the numerical studies and variations in the angle of the DW VGs, which affect the heat transfer and flow resistance. These parameters have a direct impact on the thermal–hydraulic performance and economic value of VGs installed in circular channels. Future studies can build on this research by using nanofluids and different VG configurations and channel geometries.

## 2. Model description

### 2.1 Physical Model

The numerical study was carried out by modelling three-dimensional fluid flow in a circular channel. The various VG geometries were compared at different Reynolds numbers. The VGs were placed on a flat plate in the centre of the channel in an in-line configuration, as shown in Figure 1(a); the orientation of the VGs on the flat plate is shown in Figure 1(b). The modelling characteristics refer to the simulation performed by Tian *et al.*, [20]. In total, 56 pairs of DW VGs were placed on the top and bottom surfaces of the flat plate in the circular channel, which had a hydraulic diameter of 47 mm. The distance between each VG with longitudinal and latitudinal pitch was 30 mm and 20 mm,

respectively. The angle of each VG was varied from  $90^\circ$  to  $150^\circ$  at intervals of  $15^\circ$ , with a set angle of attack of  $30^\circ$ , as shown in Figure 2. Details regarding the side sizes of the VGs are shown in Figure 3 and Table 1.

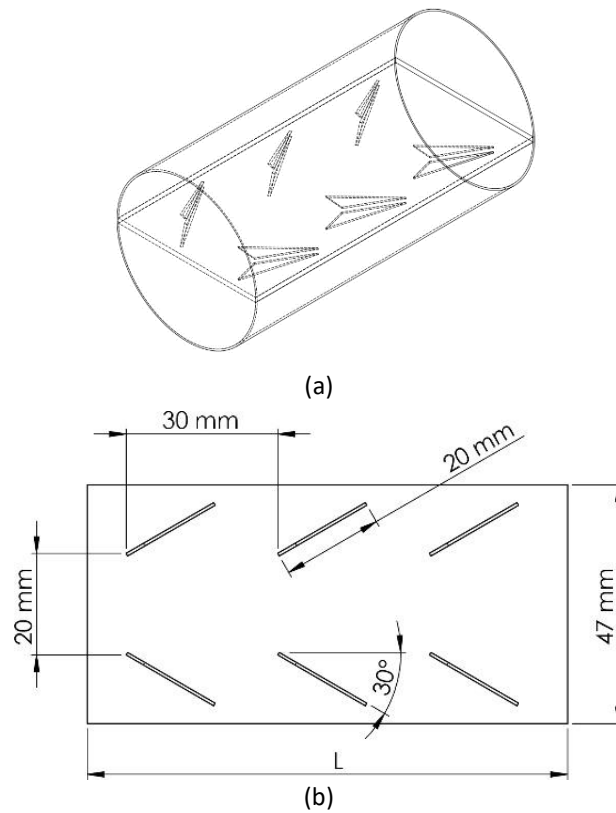


**Fig. 1.** Geometries of circular channel and flat plate with VGs: (a) isometric view of circular channel and (b) top view of flat plate

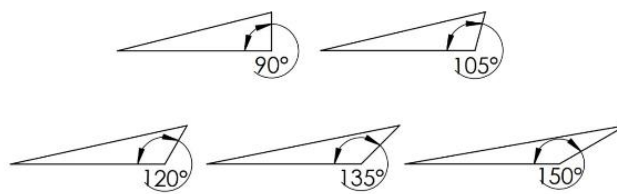


**Fig. 2.** Various angles used for VGs

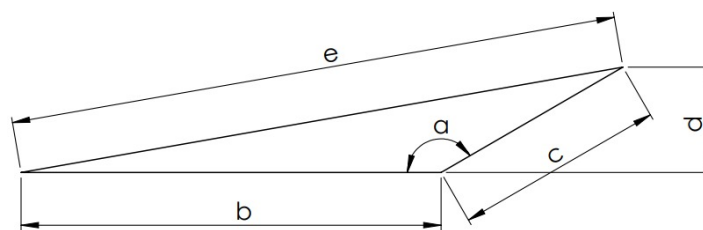


**Fig. 3.** Dimensions of VGs

**Table 1**  
DW VG side dimensions

Angle of VG ( $\alpha$ )	Side (b)	Side (c)	Side (d)	Side (e)
90°	16 mm	4 mm	4 mm	16.49 mm
105°	16 mm	4.14 mm	4 mm	17.53 mm
120°	16 mm	4.62 mm	4 mm	18.74 mm
135°	16 mm	5.66 mm	4 mm	20.40 mm
150°	16 mm	8 mm	4 mm	23.27 mm

## 2.2 Governing Equations

The flow conditions in the channel are assumed to be steady state and incompressible flow. The winglets were modelled as baffle walls with the adiabatic condition. The Reynolds number was varied from 4,000 to 12,000, which represents turbulent flow. The SIMPLE pressure–velocity coupling and the k– $\omega$  SST (shear stress transport) model were applied in this study because the Nusselt number of the k– $\omega$  SST number is close to the result of the Dittus–Boelter correlation. The equations of continuity, momentum, energy conservation, and k– $\omega$  SST can be expressed as follows.

Continuity equation:

$$\frac{\partial(Ru_R)}{R} + \frac{\partial u_\theta}{R\partial\theta} + \frac{\partial u_z}{\partial z} = 0 \quad (1)$$

Momentum equation in the direction of R:

$$\rho \left( \overline{u_R} \frac{\partial \overline{u_R}}{\partial R} + \frac{\overline{u_\theta}}{\theta} \frac{\partial \overline{u_R}}{\partial \theta} - \frac{\overline{u_\theta}^2}{R} + \overline{u_z} \frac{\partial \overline{u_R}}{\partial z} \right) = -\frac{\partial \overline{p}}{\partial R} + \mu \left( \frac{1}{R} \frac{\partial}{\partial R} \left( R \frac{\partial \overline{u_R}}{\partial R} \right) - \frac{\overline{u_R}}{R^2} + \frac{\partial^2 \overline{u_R}}{R^2 \partial \theta^2} - \frac{2}{R^2} \frac{\partial \overline{u_\theta}}{\partial \theta} + \frac{\partial^2 \overline{u_R}}{\partial z^2} \right) + \frac{\partial}{\partial \theta} (-\rho \overline{u'_R u'_\theta}) + \frac{\partial}{\partial z} (-\rho \overline{u'_R u'_z}) \quad (2)$$

Momentum equation in the direction of  $\theta$ :

$$\rho \left( \overline{u_R} \frac{\partial \overline{u_\theta}}{\partial R} + \frac{\overline{u_\theta}}{R} \frac{\partial \overline{u_\theta}}{\partial \theta} - \frac{\overline{u_\theta} \overline{u_R}}{R} + \overline{u_z} \frac{\partial \overline{u_\theta}}{\partial z} \right) = -\frac{\partial \overline{p}}{R \partial \theta} + \mu \left( \frac{1}{R} \frac{\partial}{\partial R} \left( R \frac{\partial \overline{u_\theta}}{\partial R} \right) - \frac{\overline{u_\theta}}{R^2} + \frac{\partial^2 \overline{u_\theta}}{R^2 \partial \theta^2} - \frac{2}{R^2} \frac{\partial \overline{u_R}}{\partial \theta} + \frac{\partial^2 \overline{u_\theta}}{\partial z^2} \right) + \frac{\partial}{\partial R} (-\rho \overline{u'_\theta u'_R}) + \frac{\partial}{\partial z} (-\rho \overline{u'_\theta u'_z}) \quad (3)$$

Momentum equation in the direction of z:

$$\rho \left( \overline{u_R} \frac{\partial \overline{u_z}}{\partial R} + \frac{\overline{u_\theta}}{R} \frac{\partial \overline{u_z}}{\partial \theta} + \overline{u_z} \frac{\partial \overline{u_z}}{\partial z} \right) = -\frac{\partial \overline{p}}{\partial z} + \mu \left( \frac{1}{R} \frac{\partial}{\partial R} \left( R \frac{\partial \overline{u_z}}{\partial R} \right) + \frac{\partial^2 \overline{u_z}}{R^2 \partial \theta^2} + \frac{\partial^2 \overline{u_z}}{\partial z^2} \right) + \frac{\partial}{\partial R} (-\rho \overline{u'_z u'_R}) + \frac{\partial}{\partial \theta} (-\rho \overline{u'_z u'_\theta}) \quad (4)$$

Energy conservation equation:

$$\rho C_P \left( u_R \frac{\partial T}{\partial R} + \frac{u_\theta}{R} \frac{\partial T}{\partial \theta} + u_z \frac{\partial T}{\partial z} \right) = -\lambda \left( \frac{1}{R} \frac{\partial}{\partial R} \left( R \frac{\partial T}{\partial R} \right) + \frac{1}{R^2} \frac{\partial^2 T}{\partial \theta^2} + \frac{\partial^2 T}{\partial z^2} \right) \quad (5)$$

Transport equation for k– $\omega$  SST:

$$\frac{\partial}{\partial t} (\rho k) + \frac{\partial}{\partial x_i} (\rho k u_i) = \left( \Gamma_k \frac{\partial k}{\partial x_j} \right) + \overline{G}_k - Y_k + S_k \quad (6)$$

$$\frac{\partial}{\partial t}(\rho\omega) + \frac{\partial}{\partial x_i}(\rho\omega u_i) = \frac{\partial}{\partial x_j}\left(\Gamma_\omega \frac{\partial \omega}{\partial x_j}\right) + \bar{G}_\omega - Y_\omega + D_\omega + S_\omega \quad (7)$$

### 2.3 Parameter Definitions

The main parameters considered in this study are defined as follows.

Reynolds number:

$$Re = \frac{\rho u D_h}{\mu} \quad (8)$$

Nusselt number:

$$Nu = \frac{h D_h}{\lambda} \quad (9)$$

Friction factor:

$$f = \frac{\Delta P D_h}{\frac{1}{2} \rho u^2 L} \quad (10)$$

where  $\rho$ ,  $u$ ,  $D_h$ ,  $\mu$ ,  $\lambda$ , and  $L$  are the density, intake airflow velocity, hydraulic diameter, dynamic viscosity, thermal conductivity of air, and length of the channel, respectively.

Thermal enhancement factor (TEF):

$$TEF = \frac{\frac{Nu}{Nu_0}}{\left(\frac{f}{f_0}\right)^{\frac{1}{3}}} \quad (11)$$

Cost–benefit ratio (CBR):

$$CBR = \frac{\% \Delta P}{\% Nu} \quad (12)$$

where the subscript 0 and  $\Delta P$  are the plane tube (without VG) and pressure drop conditions, respectively.

### 2.4 Boundary Conditions

The thermophysical properties of the air fluid listed in Table 2 and the boundary conditions that follow were used to solve the mathematical equations used in this study.

**Table 2**

Thermophysical properties of air fluid at 300 K

Density (kg/m <sup>3</sup> )	Dynamic viscosity (kg/m·s)	Heat capacity (J/kg·K)	Thermal conductivity (W/m·K)
1.225	1.789 × 10 <sup>-5</sup>	1006.44	0.0242

Inlet:

$$u_z = u_{z, in}; u_\theta = u_R = 0; p = p_{in}; T_{in} = 300 \text{ K} \quad (13)$$

Outlet:

$$\frac{\partial u_z}{\partial z} = 0; \frac{\partial p}{\partial z} = 0; \frac{\partial T}{\partial z} = 0 \quad (14)$$

Wall:

$$T_w = 500 \text{ K} \quad (15)$$

### 2.5 Computational Domain

The computational domain consists of an upstream extended region, the test region, and an extended downstream region. Before entering the test section, the extended upstream region is used to obtain fully developed flow [21, 22]. Subsequently, the air passes through the test section, which contains 56 pairs of the DW VGs arranged on the top and bottom surfaces of the flat plate in an in-line configuration. The surface of the circular channel is subjected to heat induction along the test section. The air passes through the extended downstream region, which helps prevent reverse flow [21, 22]. The schematic of this computational domain is shown in Figure 4.

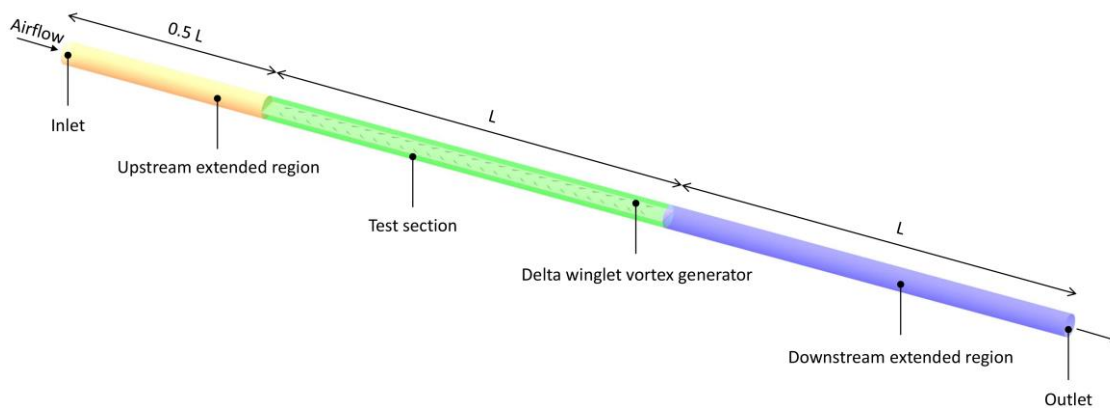


**Fig. 4.** Computational domain of the model – three-dimensional view

### 2.6 Grid Independence Test

A grid independence test was performed to determine the optimum grid for the simulation. The aim of this test is to optimise the calculation process of the computational domain [23]. The polyhedral mesh type was chosen in this study because it reduces the mesh number and speeds up calculations involving complex domain geometries [19]. The mesh size used in the test section area was 0.5 mm, as shown in Figure 5. The results of the grid independence test revealed that the optimal number of grids at  $Re = 12,000$  considering the DW VG geometry with an angle of  $150^\circ$  is 1.8 million, as shown in Figure 6.

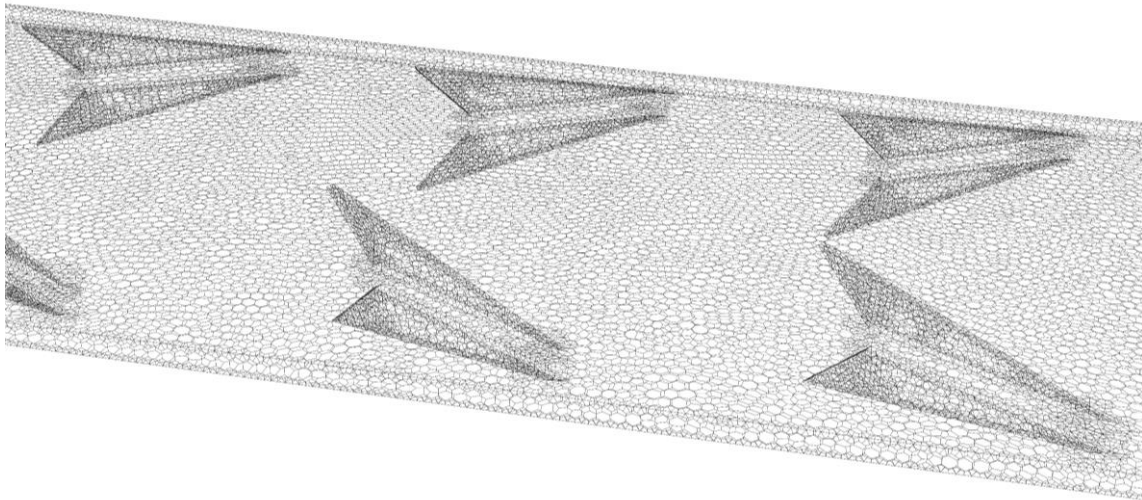


**Fig. 5.** Polyhedral mesh of the computational grid

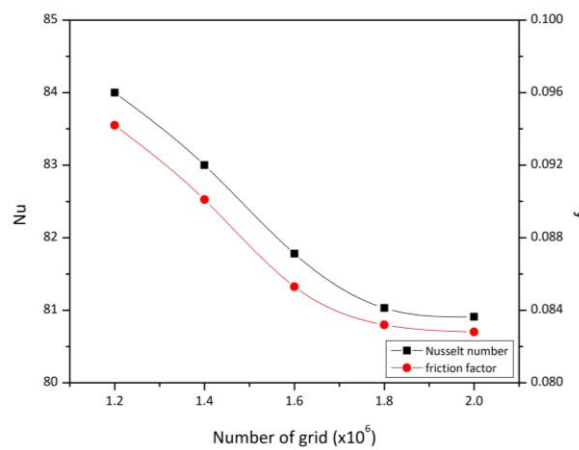


**Fig. 6.** Relationship between Nusselt number and friction factor and the number of grid cells

### 3. Numerical Methods and Validation

The SIMPLE (Semi-Implicit Method for Pressure Linked Equations) algorithm was employed to solve the pressure–velocity coupling problem. The second-order upwind scheme was used to discretise the pressure, momentum, and energy equations considering turbulent flow. The  $k-\omega$  SST (Shear Stress Transport) turbulent model was modelled with the criteria of convergence of continuity equations, velocity (X-, Y-, and Z-axes),  $k$ ,  $\omega < 10^{-5}$ , and energy  $< 10^{-8}$ .

The validation process made use of two parameters – the Nusselt number and the friction factor – considering the flow conditions with and without VGs. The Dittus–Boelter correlation for the Nusselt number and the Blasius correlation for the friction factor were applied in the plane tube condition (without VGs), as shown in Figure 7. A previous study by Tian *et al.*, [20] was used to compare the geometry of the circular channel with the air fluid between the DW VGs for validation of the second condition (with VGs), as shown in Figure 8. Both methods indicated that the two parameters have similar trends, with error deviations of 3.58% and 7.12% under each condition.

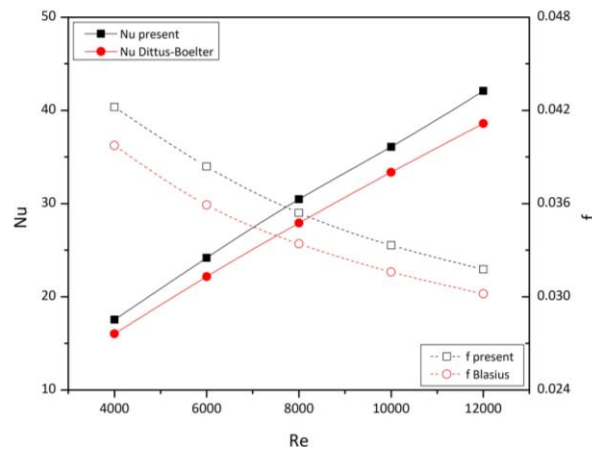


Fig. 7. Validation comparing plane tubes

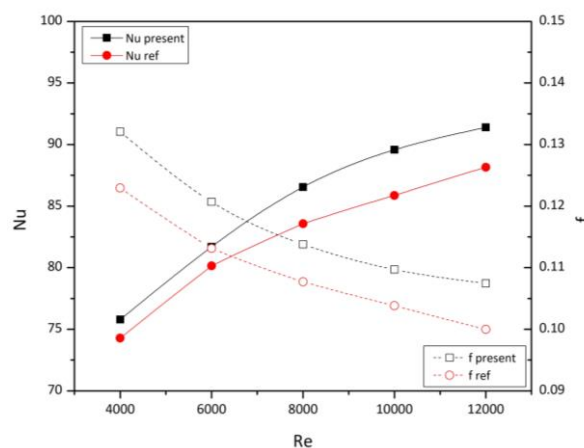
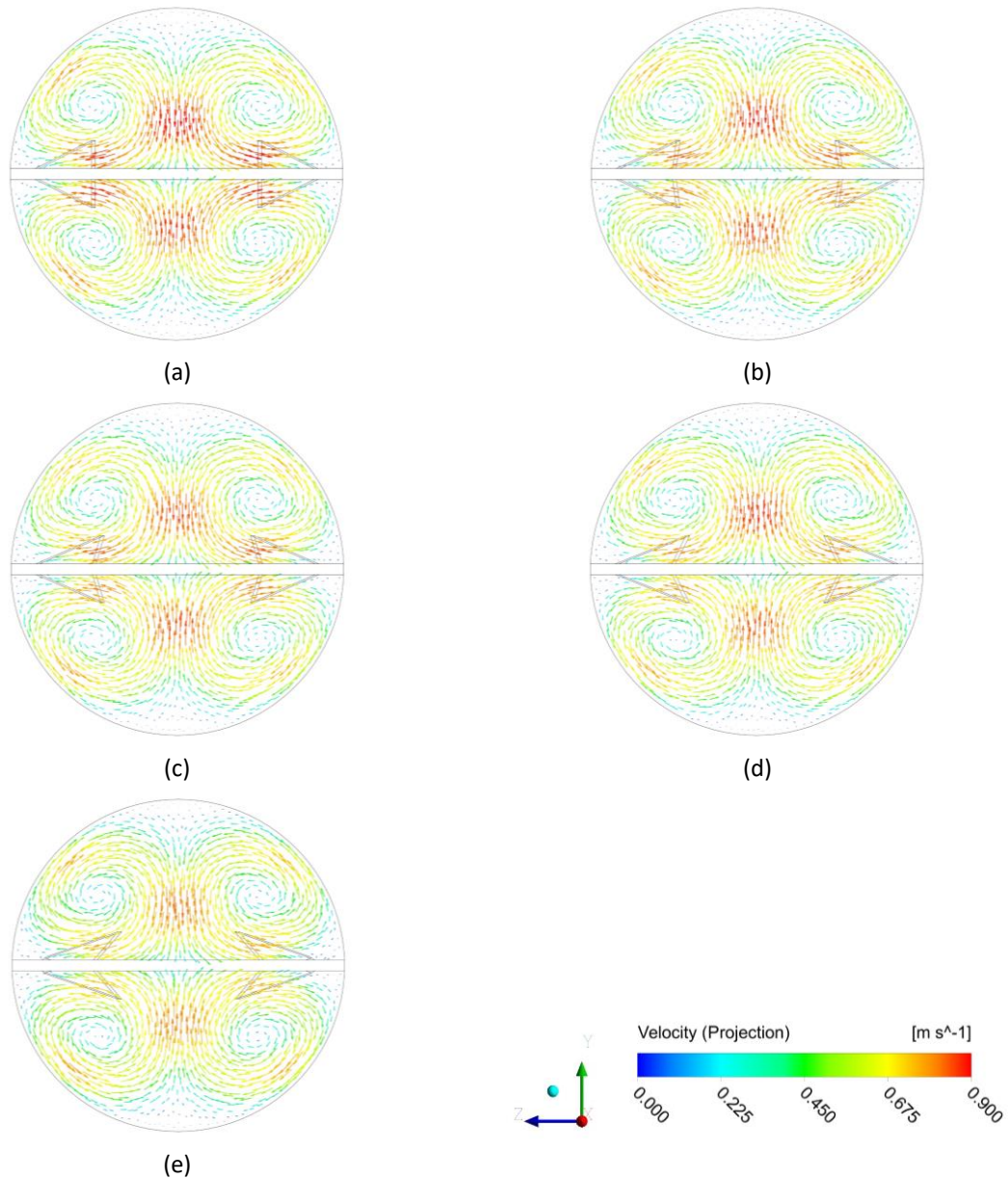


Fig. 8. Validation of Nu and f values by comparing with values obtained by Tian *et al.*, [18]

## 4. Result and Discussion

### 4.1 Flow Structures

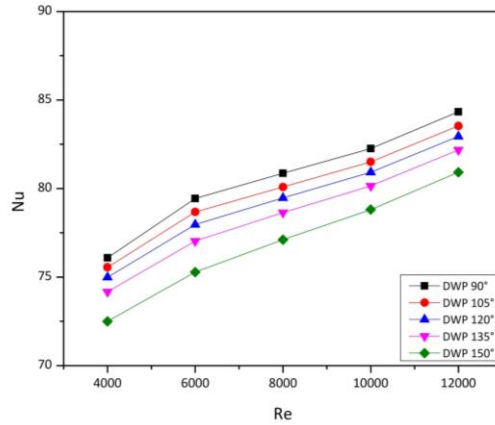
Figure 9 shows the velocity vectors in the YZ plane at  $X = 900$  mm and  $Re = 12,000$  from the inlet of the test section for DW VGs with angles of  $90^\circ$ ,  $105^\circ$ ,  $120^\circ$ ,  $135^\circ$ , and  $150^\circ$ . As shown, the velocity vector plots have common features. Four main vortices of almost the same size are visible in each case. However, the tangential velocity varies with the DW VG angle. The DW VGs with an angle of  $90^\circ$  produce the highest tangential velocity strength; the others, in decreasing order, are the DW VGs with angles of  $105^\circ$ ,  $120^\circ$ ,  $135^\circ$ , and  $150^\circ$ . This is because installing the DW VGs at an angle of  $90^\circ$  produces a stronger main vortex resulting from the downstream fluid flow above the DW VGs. The  $90^\circ$  DW VG can also generate turbulence to increase heat transfer [24]. The  $150^\circ$  DW VG produces the worst LV, as indicated by the low tangential velocity, as the VG length is considerably more than that of the  $90^\circ$  DW VG configuration.



**Fig. 9.** Velocity vectors in the YZ plane at X = 900 mm for DW VGs with angles of: (a) 90°, (b) 105°, (c) 120°, (d) 135°, and (e) 150°

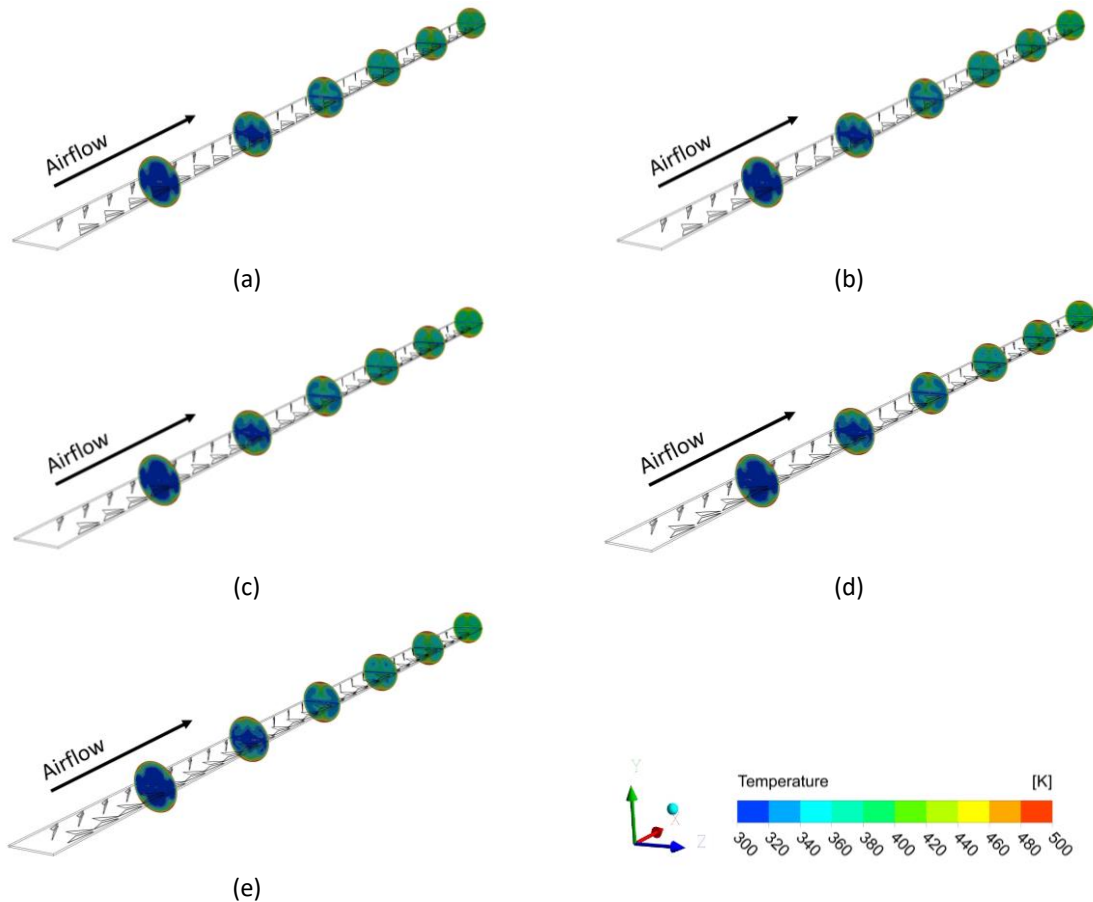
#### 4.2 Heat Transfer and Temperature Distribution

Figure 10 shows the variation in the Nusselt number with the Reynolds number at different DW VG angles. In general, the results suggest that the higher the Reynolds number, the higher the heat transfer, as indicated by the increase in the Nusselt number. Furthermore, the lower the DW VG angle, the higher the heat transfer. For example, at Re = 4,000, the heat transfer from the DW VG decreases by 0.94%, 1.65%, 2.56%, and 4.05% for angles of 105°, 120°, 135°, and 150°, respectively, compared to that with an angle of 90°. This is supported by previous research by Awais and Bhuiyan [25], who stated that a higher Reynolds number affects the amount of heat transfer. Notably, at Re = 6,000 the increase in heat transfer is higher than that at the other Reynolds numbers. Considering only the Nusselt number, this Reynolds number appears to be optimal.



**Fig. 10.** Variation in Nusselt number with Reynolds number at different DW VG angles

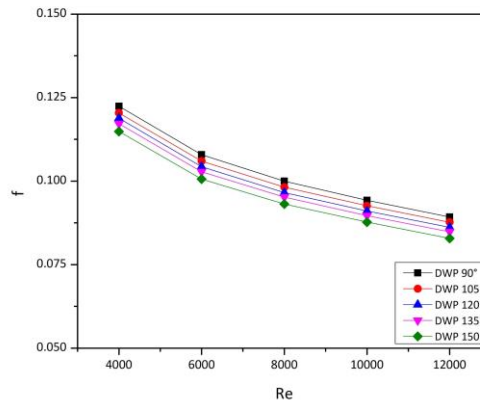
Temperature contours depicting the variation in heat transfer are shown in Figure 11. The plots are in the YZ plane at X = 150 mm, 300 mm, 450 mm, 600 mm, 750 mm, and 900 mm, and Re = 12,000. As shown in Figure 11 (a), the 90° DW VG provides effective fluid mixing compared to the other DW VGs. This is depicted by the even colour of the temperature contour, which indicates that hot and cold fluids mix and increase heat transfer in the channel [7, 25]. In contrast, as shown in Figure 11 (e), the temperature contour of the 150° DW VG appears more varied; this is also reflected in Figure 9 (e), which has the lowest tangential velocity compared to the other DW VGs.



**Fig. 11.** Temperature contours in YZ planes for DW VGs with angles of: (a) 90°, (b) 105°, (c) 120°, (d) 135°, and (e) 150°

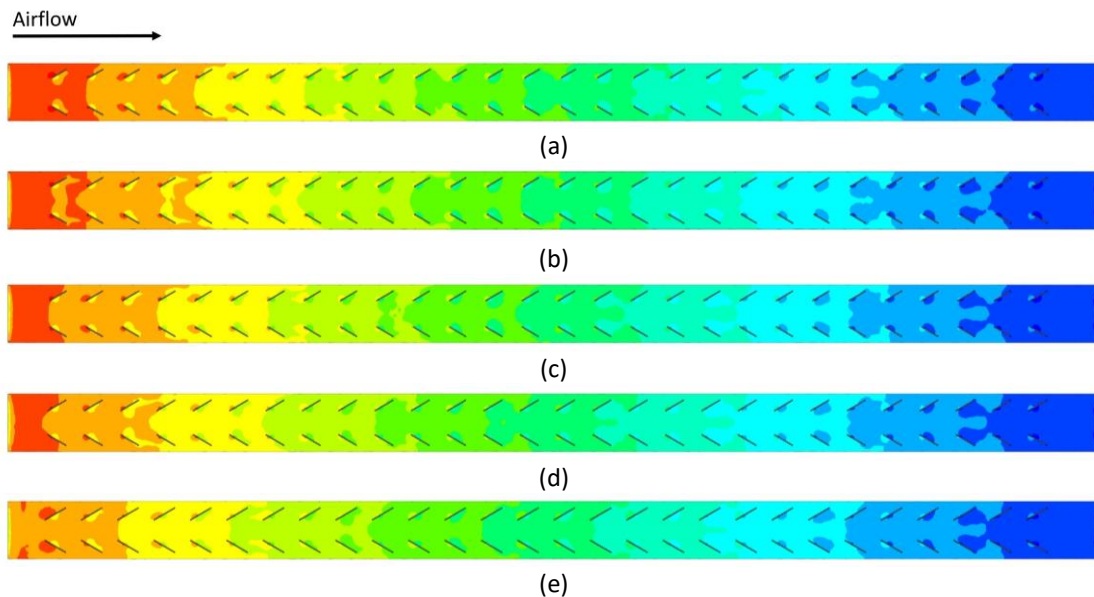
### 4.3 Flow Resistance and Pressure Drop

Figure 12 shows the variation in the friction factor with the Reynolds number, considering different DW VG angles. In general, the results suggest that the higher the Reynolds number, the lower the flow resistance in the channel, as indicated by the decrease in the friction factor. The 90° DW VG had the highest flow resistance compared to the other DW VGs. For example, at Re = 12,000, compared to the 90° DW VG, the friction factor decreased by 1.78%, 3.49%, 5.03%, and 7.18% for DW VGs with angles of 105°, 120°, 135°, and 150°, respectively.



**Fig. 12.** Variation in friction factor with Reynolds number at different DW VG angles

Figure 13 shows the pressure contours of different DW VGs at Re = 12,000. The 90° DW VG appears to have the highest pressure drop. This reflects the temperature contour shown in Figure 11 (a), as an increase in heat transfer can lead to a high pressure drop along the flow [26, 27]. This confirms that the LV produced by the DW VGs is highest at an angle of 90°, which is corroborated by the velocity vectors shown in Figure 9 (a) which have the highest velocity. At other DW VG angles, the pressure drop decreases, as does the heat transfer.



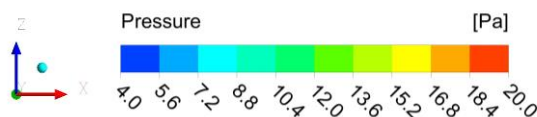


**Fig. 13.** Pressure contours along the ZX plane at  $Y = 1.5$  mm considering DW VGs with angles of: (a)  $90^\circ$ , (b)  $105^\circ$ , (c)  $120^\circ$ , (d)  $135^\circ$ , and (e)  $150^\circ$

#### 4.4 Thermal–Hydraulic Performance

The TEF was used to evaluate the thermal–hydraulic performance of the installed DW VGs with different angles. The TEF was determined by comparing the ratios of the Nusselt number and the friction factor [28, 29]. If the Nusselt number ratio exceeds the friction factor ratio, the TEF value tends to be higher. Figure 14 shows the variation in the TEF with the Reynolds number for DW VGs with angles of  $90^\circ$ ,  $105^\circ$ ,  $120^\circ$ ,  $135^\circ$ , and  $150^\circ$ . Overall, the TEF tends to decrease in all cases owing to the higher flow resistance compared to the heat transfer along the direction of flow. The DW VG with an angle of  $90^\circ$  had a mean value of 0.83% TEF, which was the highest TEF value. The TEF value of the DW VG with an angle of  $150^\circ$  was the least at all Reynolds numbers.

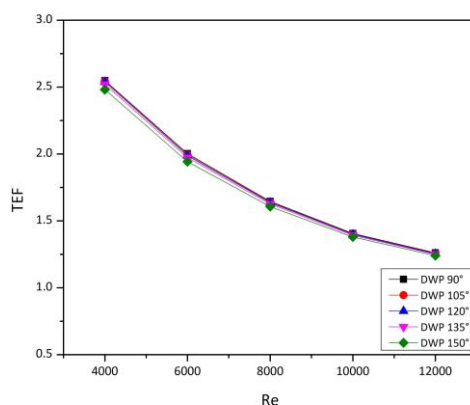


**Fig. 14.** Variation in TEF with Reynolds number at different DW VG angles

#### 4.5 Economic Value

The CBR was used to analyse the economic value of the increase in heat transfer in this study. The CBR compares the percentage increase in the pressure drop with the percentage increase in the Nusselt number considering the different DW VG configurations. A low CBR provides better thermal performance than the drag force [20]. As shown in Figure 15, the DW VG with an angle of  $150^\circ$  had the lowest CBR. On average, the DW VG with an angle of  $150^\circ$  had a 7.18% lower CBR than that with an angle of  $90^\circ$ . This is primarily because the percentage increase in the Nusselt number is higher than the pressure drop in the DW VG with an angle of  $150^\circ$ .

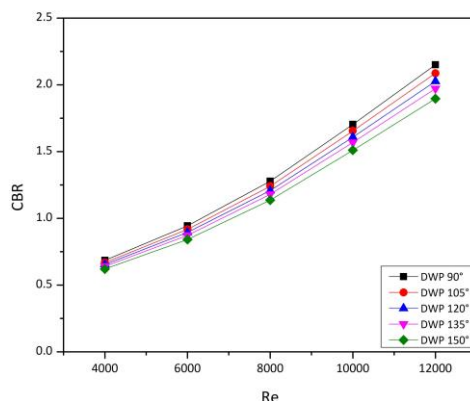


Fig. 15. Variation in CBR with Reynolds number at different DW VG angles

## 5. Conclusion

This study aimed to enhance the heat transfer and decrease the flow resistance in circular channels fitted with VG flat plates. Five different DW VG angles – 90°, 105°, 120°, 135°, and 150° – were used in this study, and the Reynolds number was varied between 4,000 and 12,000, at intervals of 2,000. The results of this study can be summarised as follows:

- i. The LV produced by the 90° DW VG at Re = 12,000 was characterised by the most uniform mixing of hot and cold fluids along the spanwise cross-section of the flow.
- ii. The installation of a 90° DW VG increases heat transfer but leads to a high flow pressure drop compared to the 150° DW VG; the heat transfer and friction factor are 84.33 and 0.089, respectively.
- iii. The best thermohydraulic performance (TEF) was obtained with the 90° DW VG (TEF = 1.64%). Furthermore, the economic value calculated using the CBR was 11.8%, which is the highest of all the configurations considered in this study.

## References

- [1] Li, L, Du, X., Zhang, Y., Yang, L., and Yang, Y. "Numerical simulation on flow and heat transfer of fin-and-tube heat exchanger with longitudinal vortex generators." *International Journal of Thermal Sciences* 92 (2015): 85-96. <https://doi.org/10.1016/j.ijthermalsci.2015.01.030>
- [2] Awais, M. and Bhuiyan, A.A. "Enhancement of thermal and hydraulic performance of compact finned-tube heat exchanger using vortex generators (VGs): A parametric study." *International Journal of Thermal Sciences* 140 (2019): 154-166. <https://doi.org/10.1016/j.ijthermalsci.2019.02.041>
- [3] Gururatana, S., Prapainop, R., Chuepeng, S., and Skullong, S. "Development of heat transfer performance in tubular heat exchanger with improved NACA0024 vortex generator." *Case Studies in Thermal Engineering* 26 (2021): 101166. <https://doi.org/10.1016/j.csite.2021.101166>
- [4] Phu, N. M. and Thao, P. B. "Thermohydraulic Performance of a Fin and Inclined Flat Tube Heat Exchanger: A Numerical Analysis." *CFD Letters* 13, no. 7 (2021): 1-12. <https://doi.org/10.37934/cfdl.13.7.112>
- [5] Fiebig, M., Valencia, A., and Mitra, N.K. "Wing-type vortex generators for fin-and-tube heat exchangers." *Experimental Thermal and Fluid Science* 7 (1993): 287-295. [https://doi.org/10.1016/0894-1777\(93\)90052-K](https://doi.org/10.1016/0894-1777(93)90052-K)
- [6] Fiebig, M. "Embedded vortices in internal flow: heat transfer and pressure loss enhancement." *International Journal of Heat and Fluid Flow* 16 (1995): 376-388. [https://doi.org/10.1016/0142-727X\(95\)00043-P](https://doi.org/10.1016/0142-727X(95)00043-P)
- [7] Fiebig, M. "Vortices, Generators and Heat Transfer." *Chemical Engineering Research and Design* 76 (1998): 108-123. <https://doi.org/10.1205/026387698524686>
- [8] Mugisidi, D., Heriyani, O., Gunawan, P.H., and Apriani, D. "Performance Improvement of a Forced Draught Cooling Tower Using a Vortex Generator." *CFD Letters* 13, no. 1 (2021): 45-57. <https://doi.org/10.37934/cfdl.13.1.4557>

- [9] Doori W.H.A.A. "Experiments and Numerical Investigations for Heat Transfer from a Horizontal Plate via Forced Convection Using Pin Fins with Different Hole Numbers." *CFD Letters* 14, no. 9 (2022): 1-14. <https://doi.org/10.37934/cfdl.14.9.114>
- [10] Tang, L.H., Chu, W.X., Ahmed, N., and Zeng, M. "A new configuration of winglet longitudinal vortex generator to enhance heat transfer in a rectangular channel." *Applied Thermal Engineering* 104 (2016): 74-84. <https://doi.org/10.1016/j.applthermaleng.2016.05.056>
- [11] Samadifar, M. and Toghraie, D. "Numerical simulation of heat transfer enhancement in a plate-fin heat exchanger using a new type of vortex generators." *Applied Thermal Engineering* 133 (2018): 671-681. <https://doi.org/10.1016/j.applthermaleng.2018.01.062>
- [12] Da Silva, F.A.S., Dezan, D.J., Pantaleao, A.V., and Salviano, L.O. "Longitudinal vortex generator applied to heat transfer enhancement of a flat plate solar water heater", *Applied Thermal Engineering* 158 (2019): 113790. <https://doi.org/10.1016/j.applthermaleng.2019.113790>
- [13] Luo, C., Wu, S., Song, K., Hua, L., and Wang, L. "Thermo-hydraulic performance optimization of wavy fin heat exchanger by combining delta winglet vortex generators." *Applied Thermal Engineering* 163 (2019): 114343. <https://doi.org/10.1016/j.applthermaleng.2019.114343>
- [14] Ke, Z., Chen, C.L., Li, K., Wang, S., and Chen, C.H. "Vortex dynamics and heat transfer of longitudinal vortex generators in a rectangular channel." *International Journal of Heat and Mass Transfer* 132 (2019): 871-885. <https://doi.org/10.1016/j.ijheatmasstransfer.2018.12.064>
- [15] Lin, Z.M., Li, S.F., Liu, C.P., Wang, L.B., and Zhang, Y.H. "Thermal and flow characteristics of a channel formed by aligned round tube bank fins stamped with curve delta-winglet vortex generators." *Thermal Science and Engineering Progress* 26 (2021): 101113. <https://doi.org/10.1016/j.tsep.2021.101113>
- [16] Luo, L., Zhao, Z., Qiu, D., Wang, S., Wang, Z., and Bengt, S. "An experimental investigation on the thermal augmentation of internal endwall in a two-pass duct using an array of delta-winglet vortex generator pair." *International Journal of Heat and Mass Transfer* 182 (2022): 122043. <https://doi.org/10.1016/j.ijheatmasstransfer.2021.122043>
- [17] Zhao, Z., Luo, L., Zhou, X., Wang, S., Wang, Z., and Sunden, B. "Analysis of enhanced turbulent heat transfer in a sharp turn channel having novel designed endwall with longitudinal vortex generator." *International Communications in Heat and Mass Transfer* 131 (2022): 105874. <https://doi.org/10.1016/j.icheatmasstransfer.2021.105874>
- [18] Perez, A.M., Altamirano, C.F.A., and Perez, R.B. "Parametric analysis of the influence of geometric variables of vortex generators on compact louver fin heat exchangers." *Thermal Science and Engineering Progress* 27 (2022): 101151. <https://doi.org/10.1016/j.tsep.2021.101151>
- [19] Syaiful, Wicaksono, T.A., Tony, M.S.K., Suprihanto, A., and Soetanto, M.F. "Heat transfer intensification with field synergy principle in a fin-and-tube heat exchanger through convex strip installation." *Engineering Reports* 4 (2022): 12510. <https://doi.org/10.1002/eng2.12510>
- [20] Tian, M.W., Khorasani, S., Moria, H., Pourhedayat, S., Dizaji, H.S. "Profit and efficiency boost of triangular vortex-generators by novel techniques." *International Journal of Heat and Mass Transfer* 156 (2020): 119842. <https://doi.org/10.1016/j.ijheatmasstransfer.2020.119842>
- [21] Syaiful, Ayutasari, A., Soetanto, M.F., Siswantara, A.I., and Bae, M.W. "Thermo-hydrodynamics Performance Analysis of Fluid Flow through Concave Delta Winglet Vortex Generators by Numerical Simulation." *International Journal of Technology* 8 (2017): 1276-1285. <https://doi.org/10.14716/ijtech.v8i7.706>
- [22] Syaiful, Hendraswari, M.P., Tony, M.S.K., and Soetanto, M.F. "Heat Transfer Enhancement inside Rectangular Channel by Means of Vortex Generated by Perforated Concave Rectangular Winglets." *Fluids* 6 (2021): 1-14. <https://doi.org/10.3390/fluids6010043>
- [23] Hamad, A., Aftab, S.M.A., and Ahmad, K.A. "Reducing Flow Separation in T-Junction Pipe Using Vortex Generator: CFD Study." *Journal of Advanced Research in Fluid Mechanics and Thermal Sciences* 44, no. 1 (2018): 36-46.
- [24] Qjan, Z., Wang, Q., and Cheng, J. "Analysis of heat and resistance performance of plate fin-and-tube heat exchanger with rectangle-winglet vortex generator." *International Journal of Heat and Mass Transfer* 124 (2018): 1198-1211. <https://doi.org/10.1016/j.ijheatmasstransfer.2018.04.037>
- [25] Awais, M. and Bhuiyan, A.A. "Heat transfer enhancement using different types of vortex generators (VGs): A review on experimental and numerical activities." *Thermal Science and Engineering Progress* 5 (2018): 524-545. <https://doi.org/10.1016/j.tsep.2018.02.007>
- [26] Li, M.J., Zhou, W.J., Zhang, J.F., Fan, J.F., He, Y.L., and Tao, W.Q. "Heat transfer and pressure performance of a plain fin with radiantly arranged winglets around each tube in fin-and-tube heat transfer surface." *International Journal of Heat and Mass Transfer* 70 (2014): 734-744. <https://doi.org/10.1016/j.ijheatmasstransfer.2013.11.024>

- [27] Syaiful, Wahyuni, T., Yudianto, B., and Sinaga, N. "Evaluation of Vortex Generators in the Heat Transfer Improvement of Airflow through an In-Line Heated Tube Arrangement." *Fluids* 6 (2021): 1-17. <https://doi.org/10.3390/fluids6100344>
- [28] Sun, Z., Zhang, K., Li, W., Chen, Q., and Zhen, N. "Investigations of the turbulent thermal-hydraulic performance in circular heat exchanger tubes with multiple rectangular winglet vortex generators." *Applied Thermal Engineering* 168 (2020): 114838. <https://doi.org/10.1016/j.applthermaleng.2019.114838>
- [29] Manjunath, M.S. and Fernandes, D.V. "Numerical investigation of heat transfer and friction factor characteristics of circular tube fitted with an array of semi-elliptical vortex generator inserts." *Cogent Engineering* 8 (2021). <https://doi.org/10.1080/23311916.2021.1968742>